Application of Electro-Rheological Fluids for Conveying Realistic Haptic Feedback

Conference Paper · October 2018

CITATION
1

READS
51

3 authors, including:

Alex Mazursky
Miami University
6 PUBLICATIONS **7** CITATIONS
SEE PROFILE

Tae-Heon Yang
Korea Research Institute of Standards and Science
42 PUBLICATIONS **247** CITATIONS
SEE PROFILE

Application of Electro-Rheological Fluids for Conveying Realistic Haptic Feedback

Alex Mazursky[1], Jeong-Hoi Koo[1*], and Tae-Heon Yang[2]

[1]Department of Mechanical and Manufacturing Engineering, Miami University, Oxford, OH, 45056, USA

[2]Department of Electronic Engineering, Korea National University of Transportation, Chungju-si, Chungbuk, 27469, Republic of Korea

Abstract

For a device to convey realistic haptic feedback, two touch sensations must be present: tactile feedback and kinesthetic feedback. Tactile feedback consists of the sensations felt at the surface of one's skin and just underneath it, while kinesthetic feedback is felt in one's joint and muscle nerves and provides information about position and movement. Though many haptic devices today convey tactile feedback through vibrations, most neglect to integrate kinesthetic feedback. To address this issue, this study investigates a haptic device with the aim of conveying both kinesthetic and vibrotactile information to users. To this end, a prototype device based on Electro-Rheological (ER) fluids was designed and fabricated. By controlling the ER fluid flow with the use of varying electric field strengths, the device can generate various haptic sensations. The design focused around an elastic membrane that acts as seal and the actuator's contact surface. Moreover, the control electronics and structural components were integrated into a compact printed circuit board to miniaturize the device. The device was then tested using a dynamic mechanical analyzer (DMA) to evaluate its performance. During the experimental evaluation, the actuator's resistive force along with the indented depth up to 1 mm were measured by varying the input voltage magnitude, frequency, as well as wave profiles. The results indicate that a range of possible force (kinesthetic) and vibrational (tactile) sensations were produced based on input voltage signals. According to the Just-Noticeable Difference (JND) analysis, this range is sufficient to transmit distinct kinesthetic and vibrotactile sensations to users, indicating that the ER haptic device is capable of conveying realistic haptic feedback.

1. INTRODUCTION

In recent years, mobile devices have experienced a shift from mechanical buttons to smooth, touch screen keyboards. However, the benefit of larger and more versatile screens comes at a cost to the physical feedback associated with indenting buttons. The information conveyed to the user through these touch sensations is referred to as haptic feedback. In addition to visual and auditory sensations, being

* koo@miamioh.edu, Phone number: +1-513-529-0723

able to touch, feel and manipulate objects in an environment, whether real or virtual, offers the user a greater sense of immersion (Srinivasan and Basdogan, 1997). Therefore, haptic feedback is desired for numerous applications including simulators, teleoperation, entertainment and more (Coles et al., 2011; Laycock and Day, 2003; Park and Khatib, 2006). To emulate and restore physical feedback in electronics, haptic technologies are being investigated and applied to bridge the gap between the user and the virtual world. Comprehensive haptic feedback is comprised of two components: (1) kinesthetic feedback and (2) tactile feedback. Kinesthetic feedback provides information about position and movement of joints and muscles. Tactile feedback consists of the sensations felt at the surface of one's skin and just underneath it. When examining an object, humans may rub it to feel its texture and roughness (tactile sensation) and press it to feel its resistance and elasticity (kinesthetic sensation). Therefore, both sensations must be present to completely observe an object through touch (Srinivasan and Basdogan, 1997).

Although the implementation of miniature vibrotactile actuators has been extensive, the development of small-scale kinesthetic actuators has been relatively slow. Research toward kinesthetic devices generally uses alternating current/direct current (AC/DC) motors as the working principle to generate force feedback sensations (Bianchi et al., 2009; Fujita and Ohmori, 2001; Song et al., 2005). However, AC/DC motor-based actuators cannot be easily integrated into mobile devices due to their size and power consumption. Furthermore, active-controlled motors have been found to have issues with instability, making certain haptic applications less feasible (Adams et al., 1998; An and Kwon, 2006).

To avoid the problems associated with AC/DC motors, many researchers have investigated actuating haptic sensations through the adjustable properties of smart materials, such as magnetorheological (MR) fluid (An and Kwon, 2002; Jansen et al., 2010b; Kim et al., 2016). However, reducing the size of MR fluid-based actuators proves difficult due to the size required of electromagnet coils. To investigate the feasibility of miniaturizing MR fluid-based haptic devices, Yang et al. (2010) proposed a new tunable stiffness display. In subsequent parametric modeling studies, this design was reduced into a miniature button capable of producing a wide range of kinesthetic and vibrotactile feedback (Ryu et al., 2015; Yang et al., 2017). However, basing an actuator around MR fluid requires precise manufacturing to miniaturize the complex circuitry due to the solenoid coil.

Electrorheological (ER) fluid, MR fluid's counterpart with a viscosity dependent upon electric field, presents opportunity to address the difficulties of implementing MR fluid in miniature applications. Similar to MR fluid, ER fluid features response times in the order of milliseconds, low power consumption and few issues with stability (Bullough et al., 1993; Han et al., 2000; Whittle et al., 1996). Additionally, with Wen et al.'s (2003) fabrication and modeling of giant ER (GER) fluid, GER fluid-based devices are capable of producing high yield stresses, similar in order to those of MR fluid-based designs. However, compared to MR fluid, the electrical design for controlling ER fluid is simpler; only two electrodes spaced approximately 1 mm apart are needed, thinner than the equivalent solenoid coil for MR devices. With a goal of actuator mobility, a basis of ER fluid allows for smaller and more portable designs.

While ER fluid has often been applied to exclusively tactile or force feedback devices, research toward comprehensive haptic devices is limited (Fricke, 1993; Monkman, 1992; Pfeiffer et al., 1999; Taylor et al., 1996). Among these, no designs focus specifically on ER fluid's potential for device minimization. Mazursky et al. (2018) validated this idea experimentally with a small haptic button (14.5 mm thickness) based on ER fluid in flow mode driven by an elastic contact surface. However, this study left room to further reduce the actuator's size and verify its performance mathematically. In the past half-century, several mathematical models have been proposed to approximate the ER fluid's output force based on operating mode, such as flow, shear, and squeeze modes (Burton et al., 1996; Choi and Choi, 1999; Phillips, 1969; Wereley and Pang, 1998). These models are based upon the Bingham plastic behavior of ER fluid. In the current study, a pressure-driven flow mode model is presented to characterize the behavior of the proposed haptic actuator.

This study presents a new design for a miniature haptic actuator to overcome the challenges of decreasing the size of kinesthetic devices for mobile integration. The goals of this paper are to design an ER fluid based haptic actuator, to investigate its performance with mathematical modeling, and to experimentally evaluate its ability to produce both kinesthetic and tactile feedback. The actuator is manufactured using printed circuit boards (PCB) to integrate its electrical and structural components.

Within the actuator, ER fluid provides the variable resistive force to the button's kinesthetic interface. By supplying high voltage signals to the electrodes on the PCB, the device's force feedback is controlled. Introducing a frequency into the applied voltage results in oscillations in the kinesthetic response to produce a vibrotactile response. Therefore, the proposed ER fluid-based device is capable of producing haptic feedback. The next section explains the design methodology and working principles, followed by the fabrication of the prototype. Following the design section, the process of analyzing the device's behavior through math modeling is described. The experiments to measure the force profile over the actuator's stroke are then described in the experimental setup, followed by the experimental results and discussion.

2. PROPOSED DESIGN FOR A HAPTIC ACTUATOR

To design the proposed haptic actuator, the working principles of using ER fluid to produce haptic feedback were established and are first detailed in this section. The structural design of the actuator is then proposed. Finally, the fabricated prototype actuator is presented.

2.1 Working Principles

Figure 1 illustrates the cross-section and the working principle of the proposed haptic actuator. When pressing the actuator's flexible contact surface, ER fluid flows radially outward through the gap between stationary electrodes, or the activation region. Therefore, it can be said that the actuator operates in pressure-driven flow mode. To compensate for the change in volume due to indentation, radial slots have been included in the upper PCB and cover, allowing the membrane in the slots to expand elastically, creating a reciprocating reservoir (see Figure 1b). When pressure on the contact surface is released, the fluid is pushed by the contracting membrane from the reservoir and the device returns to its pre-contact state. When a voltage is applied to the electrodes, the ER fluid in the resultant electric field forms a fibrous network parallel to the field lines. This liquid-solid transition generates a yield stress with magnitude corresponding to the supplied voltage. Therefore, the force felt by the user's finger when pressing directly corresponds to the yield stress produced by the fluid. For a range of supplied voltage magnitudes and frequencies, a range of feedbacks may be felt by the user.

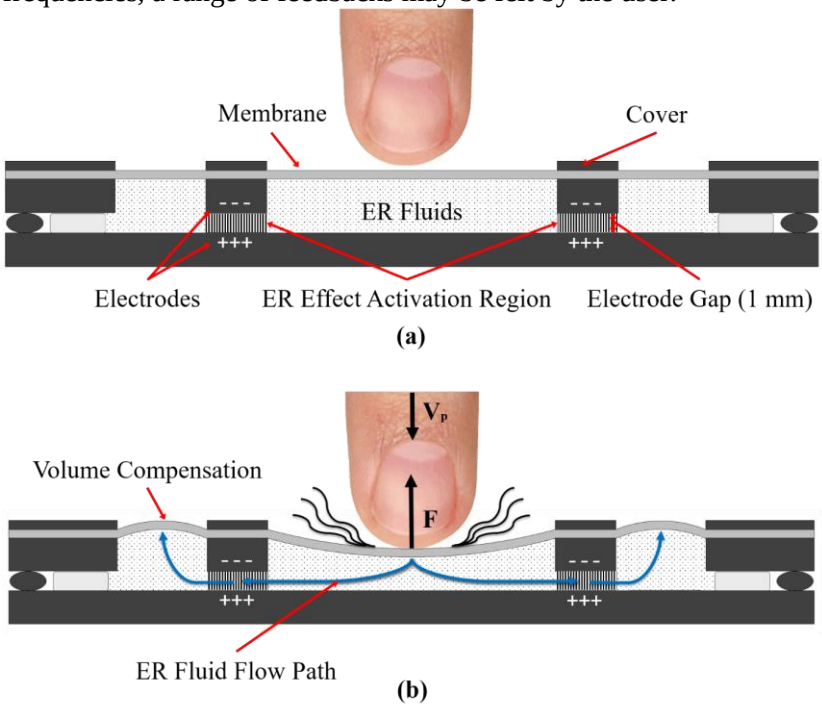

Figure 1. Working principle of the proposed haptic actuator (a) before contact and (b) mid-contact.

2.2 Design and Fabrication of a Prototype Actuator

An exploded view of the proposed haptic actuator is presented in Figure 2. The button-type actuator is comprised of two electrode PCBs, a plastic spacer and O-ring, a thin film silicone membrane and a plastic cover. The internal volume of the device contains about 1.8 mL of giant ER fluid, thus providing potential for greater yield stresses than conventional ER fluid. The bottom PCB has an annulus shaped electrode and is treated with a thin polyimide film to prevent arcing at high voltages (HV PCB). The top PCB has identical electrode geometry to the HV PCB and functions as grounding (GND PCB) for the applied electric field. The electrodes' inner and outer radii measure 7.5 and 11 mm, respectively. A plastic spacer is fitted between the two PCBs, providing rigidity to the O-ring seal and sets the gap distance between the electrodes to 1 mm. A compliant silicone membrane is sealed by a thin layer of acrylic tape to the top of the GND PCB and functions as the device's contact surface. Nylon nuts and bolts fasten the device and compress the O-ring and membrane seals to secure the ER fluid inside. Two tabs allow for HV and GND leads to be secured to the electrode PCBs for electrical inputs. The maximum indentation depth, or stroke, of the actuator is 1 mm. The assembled device measures 42 mm in diameter and 5.4 mm thick. The device was designed and manufactured with a goal of minimizing thickness to convey kinesthetic and tactile feedback in miniature applications. The size of the proposed actuator is significantly thinner than previous designs utilizing smart materials (Jansen et al., 2010a; Mazursky et al., 2018; Ryu et al., 2012; Xu et al., 2018). Additionally, the design is mechanically simple and easily controllable.

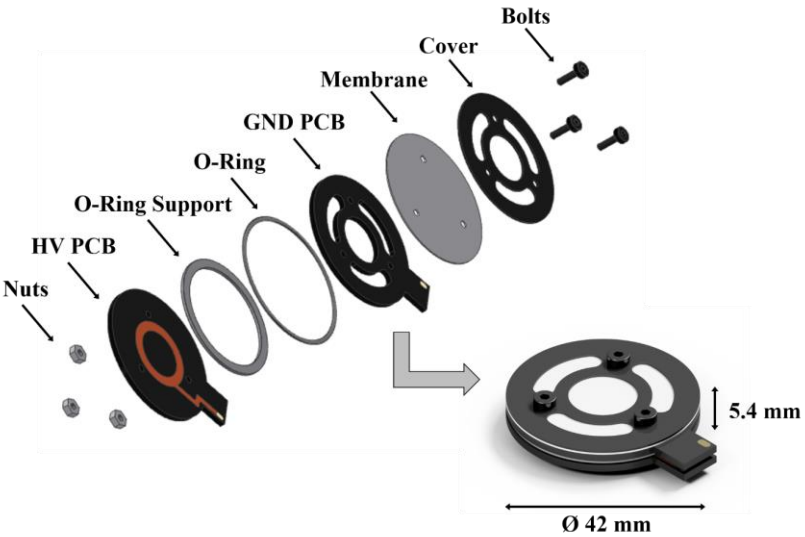

Figure 2. Exploded view drawing of the proposed haptic actuator.

3. MATHEMATICAL MODELING

To understand the actuator's performance from a mathematical perspective, a model was developed based on the actuator's fundamental behavior. First, an analytical solution to the resistive force produced by the actuator over its stroke as a function of applied electric field was derived. A numerical approach was taken to simulate the actuator's resistive force output and is presented as well.

3.1 Analytical Modeling of ER Fluid

To characterize the behavior of the proposed haptic actuator, an analytical model was developed to determine the resistive force produced by the actuator. First, boundary conditions are applied to the Navier-Stokes equation, resulting in the velocity profile of the fluid flow between the plates. Integrating about the electrode area returns the total flow rate. From the volume continuity condition, the flow rate between the plates must be equal to the flow rate due to the indenter; therefore, the pressure gradient may be realized. The pressure gradient is then used to attain the pressure drop across the plates and the contribution of the ER fluid to the resistive force produced by the actuator. Further detail to each of these steps is provided with mathematical representations in sub-subsections 3.1.1-5 below.

3.1.1 Navier-Stokes Equation and Assumptions

Upon indenting the contact membrane at a rate of V_p, ER fluid flow develops between the parallel electrodes. As shown in Figure 4, the velocity profile in the activation region is composed of three regions due to the Bingham plastic behavior of ER fluid. Flow near the electrode walls (regions 1 and 3) is where the shear stress is greatest and where yield occurs ($|\tau| > \tau_y$). Near the center of the gap (region 2, also known as the plug or core), unyielded fluid flows with a uniform velocity. A parallel plate approximation is made to estimate the annular electrodes as a rectangular duct (Wereley and Pang, 1998).

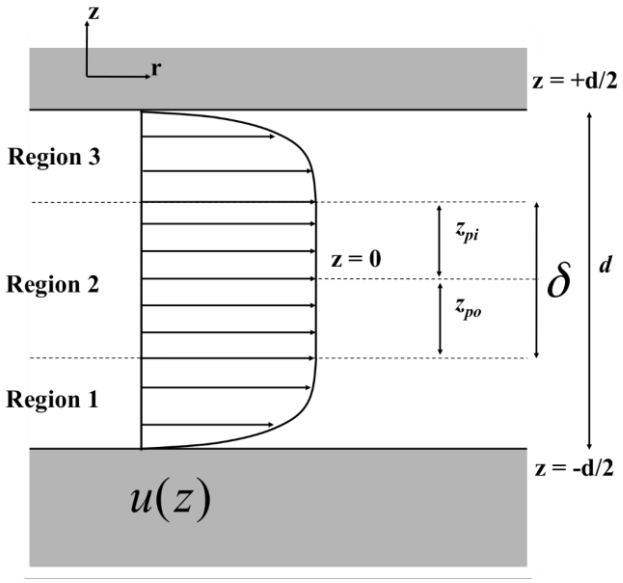

Figure 4. Velocity profile of ER fluid in the activation region associated with a fixed electrode configuration.

To find the velocity profile $u(z)$ in flow mode, the Navier-Stokes equation of motion in rectangular coordinates along the x-direction is given:

$$\rho\left(\frac{\partial u}{\partial t}+u\frac{\partial u}{\partial x}+v\frac{\partial u}{\partial y}+w\frac{\partial u}{\partial z}\right)=-\frac{dP}{dx}+\rho g_x+\mu\left(\frac{\partial^2 u}{\partial x^2}+\frac{\partial^2 u}{\partial y^2}+\frac{\partial^2 u}{\partial z^2}\right) \tag{1}$$

Applying assumptions of steady flow, unidirectional flow, mass conservation, and omitting gravity leads to the simplified relation between pressure gradient and flow profile:

$$\frac{dP}{dx}=\mu\frac{d^2u}{dz^2} \tag{2}$$

To better illustrate the physical relation to the actuator design, the variable x is renamed to r.

3.1.2 Boundary Conditions and Flow Velocity u in Each Region

To find the flow velocity in each region, integration is performed and constants are determined by applying boundary conditions (no-slip, uniform flow in region 2):

$$\begin{aligned} u_1&=\frac{1}{2\mu}\frac{dP}{dr}\left[\left(z+z_{po}\right)^2-\left(\frac{d}{2}-z_{po}\right)^2\right] \\ u_2&=-\frac{1}{2\mu}\frac{dP}{dr}\left(\frac{d}{2}-z_{pi}\right)^2 \\ u_3&=\frac{1}{2\mu}\frac{dP}{dr}\left[\left(z-z_{pi}\right)^2-\left(\frac{d}{2}-z_{pi}\right)^2\right] \end{aligned} \tag{3}$$

3.1.3 Total Flow Rate Q

Knowing $u(z)$, volumetric flow rate Q across the electrode area A may be found using:

$$Q = \int_{2\pi r_0}^{2\pi r_1} \int_{-\frac{d}{2}}^{\frac{d}{2}} (u) dz dr \tag{4}$$

where r_1 and r_0 are the outer and inner electrode radii, respectively. This integration is performed separately for each region:

$$\begin{aligned} Q_1 &= \frac{\pi}{12\mu}\frac{dP}{dr}(d-\delta)^3(r_0-r_1) \\ Q_2 &= \frac{\pi\delta}{4\mu}\frac{dP}{dr}(d-\delta)^2(r_0-r_1) \\ Q_3 &= \frac{\pi}{12\mu}\frac{dP}{dr}(d-\delta)^3(r_0-r_1) \end{aligned} \tag{5}$$

Knowing that Q_{total} is the sum of the regional flow rates and simplifying yields:

$$Q_{total} = Q_1 + Q_2 + Q_3 = \frac{\pi}{12\mu}\frac{dP}{dr}(d-\delta)^2(2d+\delta)(r_0-r_1) \tag{6}$$

3.1.4 Pressure Gradient *dP/dr*

To solve for the pressure gradient, the conservation of incompressible mass flow rate condition is utilized:

$$Q_{total} = Q_p \tag{7}$$

where $Q_p = V_p A_p$ is the flow rate due to the membrane's displacement and area of the indenter, A_p, is a function of indentation depth. Substituting into Equation 6:

$$V_p A_p = \frac{\pi}{12\mu}\frac{dP}{dr}(d-\delta)^2(2d+\delta)(r_0-r_1) \tag{8}$$

To reduce the unknown quantities, the plug thickness δ must be derived. Examining the hydrostatic force balance on a volume element and simplifying yields:

$$\delta = -\frac{2\tau_y}{dP/dr} \tag{9}$$

Additionally, for the given geometry, the pressure differential may be written as:

$$\frac{dP}{dr} = -\frac{\Delta P}{r_1 - r_0} \tag{10}$$

Substituting Equations 9 and 10 into Equation 8 results in the equation of pressure gradient:

$$V_p A_p = \frac{\Delta P}{12\mu}\left(2d - \frac{2\tau_y(r_0-r_1)}{\Delta P}\right)\left(d + \frac{2\tau_y(r_0-r_1)}{\Delta P}\right)^2 \tag{11}$$

3.1.5 Resistive Force *F*

Finally, to determine the resistive force felt by the user due to the flow mode of the ER fluid, the pressure drop across the electrodes is multiplied by the area of the indenter:

$$F = \Delta P A_p \tag{12}$$

For a membrane-based contact surface, the indenter or finger area varies with depth, resulting in a nonlinear volumetric flow rate. Therefore, the volumetric flow may be approximated:

$$A_p = \pi r_{pf}^2 \frac{d_i}{d_f} \tag{13}$$

where r_{pf} is the final radius of the indenter. The dimensionless d_i/d_f term compares the current indentation depth to the final depth.

The resistive force represented by Equation 12 only accounts for the force due to the ER fluid's dynamics. When a user interacts with and indents the proposed button-type actuator, additional resistive forces are present due to the spring force of the contact membrane and reciprocating membrane at a given depth. The membrane's elasticity was experimentally measured and a representative quadratic equation was incorporated into the model. Additionally, the force due the fluid may be separated into its active and passive components. Therefore, the kinesthetic feeling felt by the user may be represented by:

$$F_{total} = F_{ER\,Effect} + F_{0V} + F_{membrane} \quad (14)$$

By changing the magnitude and frequency of the input voltage, the magnitude of the ER effect, and therefore resistive force, can be controlled in real time resulting in a range of kinesthetic and vibrotactile sensations.

3.2 Numerical Evaluation of the Proposed Actuator

To simulate the actuator's behavior, a MATLAB® script was developed based on the modeling presented in section 3.1 to calculate the forces produced over the actuator's stroke. A coupling between the applied electric field and the giant ER fluid's yield stress was established using properties provided by the manufacturer (Smart Materials Laboratory Ltd., Hong Kong), such as a maximum yield stress of 80 kPa at 5 kV/mm, and was represented with the GER scaling function (Vemuri et al., 2012). The yield stress due to the electric field is used as an input to determine the ER actuator force. Parameters critical to the numerical results are provided below in Table 1 and reflect the properties of the fabricated prototype actuator and the experimental test setup.

Table 1 Parameters of the proposed haptic actuator.

Parameter	Symbol	Value
Electrode Gap	d	1 mm
Electrode Radius (Inner)	r_0	7.5 mm
Electrode Radius (Outer)	r_1	11 mm
Viscosity of GER Fluid	μ	0.060 Pas
Diameter of Indenter	D_p	11.8 mm
Velocity of Indentation	V_p	1 mm/s

The simulation takes applied voltage and frequency as inputs and produces plots of the force generated by the actuator along its indentation stroke. Figure 5a shows the force profiles predicted by the simulation when subjected to DC voltage inputs of 0, 1, 2, 3, and 4 kV. As shown, when no power is supplied to the actuator (0 kV, or off-state), the maximum force produced is about 2.5 N at the bottom of the stroke. When the maximum voltage is supplied (4 kV DC), the maximum force increases to nearly 3.6 N. Figure 5b shows the force profiles predicted when the model is subjected to sinusoidal excitation between 0 V and 1, 2, 3, and 4 kV at a frequency of 5 Hz. It is seen that as the magnitude of the voltage increases, the amplitude of vibration increases. Therefore, the simulation implies that the design is capable of providing both kinesthetic and vibrotactile feedback.

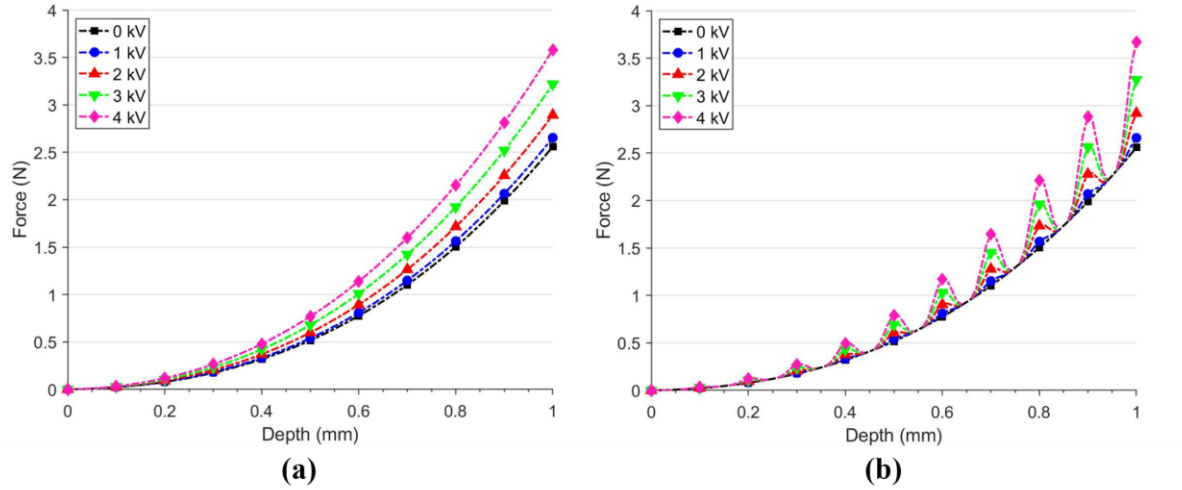

Figure 5. Results of the simulated actuator: Force (N) vs. Depth (mm) along its stroke when subjected to (a) various DC voltages and (b) 5 Hz sine functions.

4. EXPERIMENTAL EVALUATION

This section presents the experimental methods for testing the fabricated haptic device and analysis of the experimental results. The goal of the experimental analysis is to measure the device's ability to produce a significant range of kinesthetic and vibrotactile sensations. An experimental method of measuring the actuator's output with respect to depth for voltage inputs is described.

4.1 Experimental Setup

To evaluate the performance of the fabricated haptic actuator, mechanical analysis was conducted using a dynamic mechanical analyzer (RSA3, TA Instruments), function generator and voltage amplifier, as shown in Figure 6. This experimentation precisely measured the total resistive force with respect to indentation depth over the device's 1 mm stroke. The performance was evaluated under different input voltage and frequency conditions using an indenter similar in size to a human finger. An indentation rate of 1 mm/s was used.

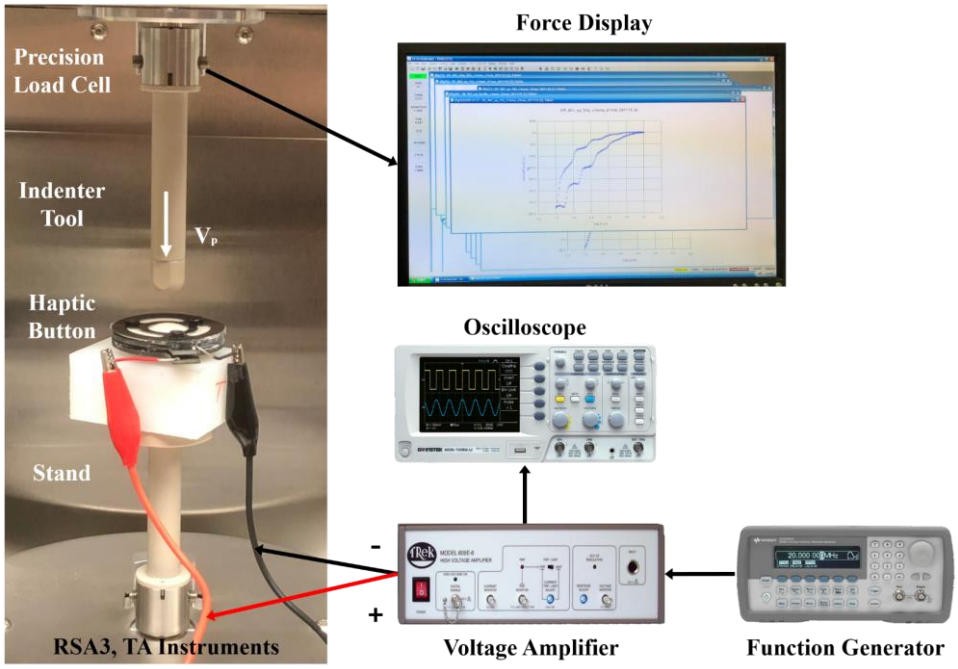

Figure 6. Experimental setup to measure the force generated by the prototype actuator with respect to indentation depth for applied voltage signals.

4.2 Kinesthetic Response

To test the actuator's ability to produce a range of stiffnesses, the actuator's resistive force was first measured in its off-state. Then, a high frequency square wave was applied between 0 V and peak amplitudes of 1, 2, 3 and 4 kV to emulate a pulsating DC signal. These results are presented below in Figure 7. As evidenced in the figure, as the magnitude of the input voltage and pressed depth increase, the resistive force increases. The off-state resistive force was measured to be about 2.5 N at maximum depth. The maximum force produced was about 3.6 N under 4 kV load. While the force profiles formed by voltages up to 3 kV had similar curvature, the force curve produced under the 4 kV input included a steep increase and decrease in force during the 0.3-0.5 mm range of the stroke. This can be attributed to a build-up of pre-yield ER fluids in the activation region, followed by a rapid yielding event.

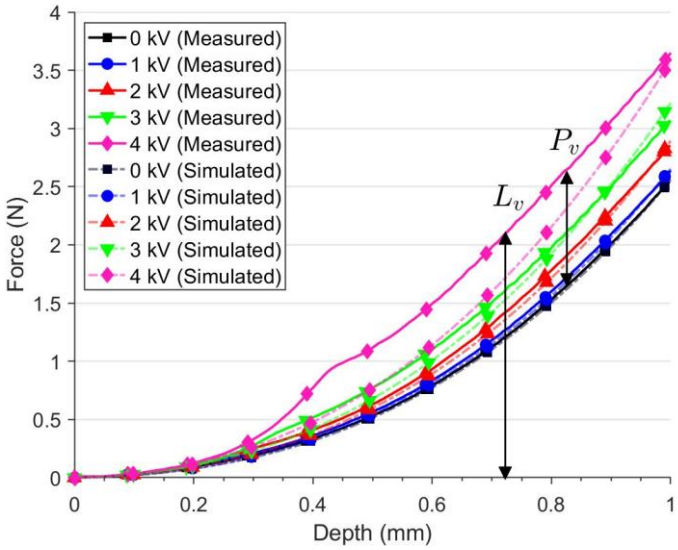

Figure 7. Comparison of kinesthetic feedback between the measured force and simulated force.

Additionally, Figure 7 compares the experimental results (opaque, smooth lines) with the results of the kinesthetic numerical simulation (transparent, dashed lines). The simulation and experimental results agree acceptably well. The off-state, 1 kV, 2 kV and 3 kV results overlay with few differences. The 4 kV responses differ due to the yielding event observed in experiments not being included in the model. However, the maximum force produced by the actuator was accurately determined by the mathematical model.

To further examine the results from a haptic perspective, the just noticeable difference (JND) must be calculated. The JND is a measure of the amount that the kinesthetic force must change for a difference to be perceived by a human. For kinesthetic feedback, force rate (Q_v) is the metric for JND and is defined as the ratio of the difference between the maximum and minimum force (P_v) to the maximum force (L_v). Performing this operation yields peak force rates of 13.5%, 23.0%, 36.3%, and 58.5% for the 1, 2, 3, and 4 kV excitations, respectively. The threshold JND for which humans can consistently detect changes in force is about 7-10% for forces between 0.5 and 200 N (Pang et al., 1991). Therefore, the proposed actuator is capable of conveying various distinguishable kinesthetic feedbacks.

4.3 Tactile Response

To demonstrate a vibrotactile response, sinusoidal voltage inputs were applied between 0 V and peak amplitudes of 1, 2, 3, and 4 kV and at frequencies of 1, 3, 5, and 10 Hz. Figure 8 presents the resultant force profiles for each set of frequencies and voltages. As seen in the figure, the force feedback responds harmonically when subjected to sinusoidal voltages. As the magnitude of the applied voltage increases, the amplitude of vibration increases as well. These results show that the actuator can convey controllable resistive forces over a range of frequencies. Therefore, the actuator is capable of communicating vibrotactile feedback.

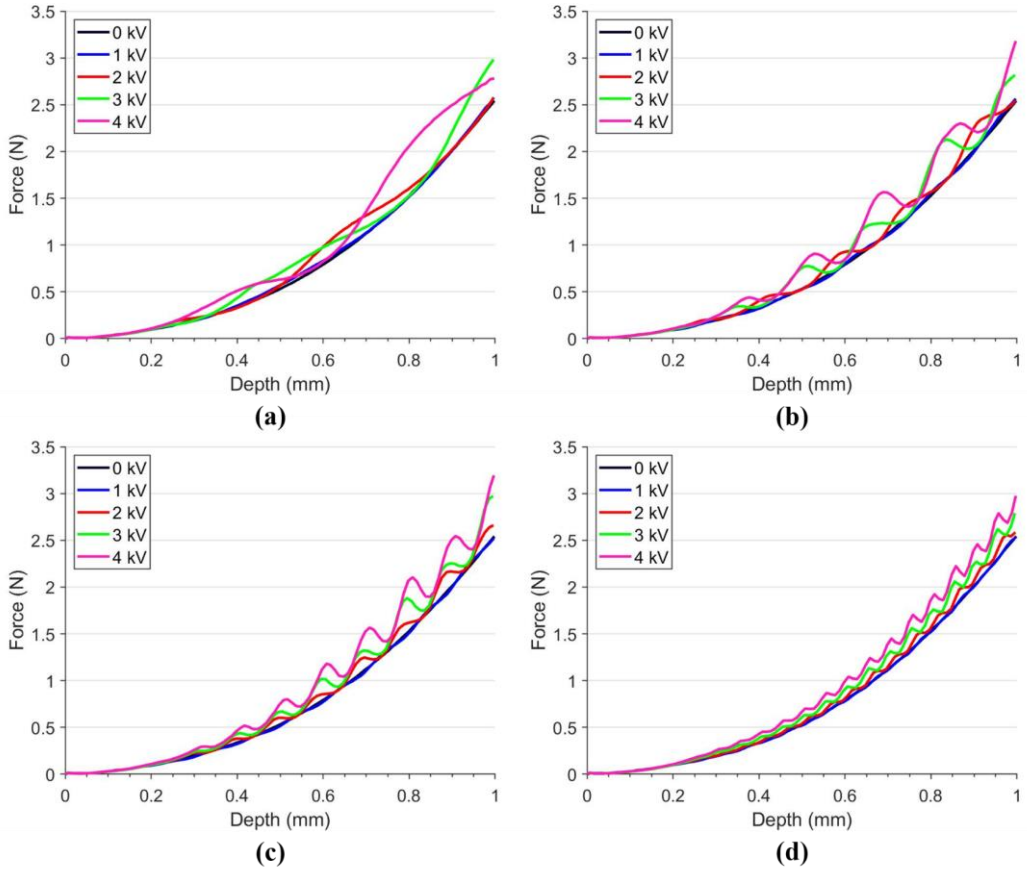

Figure 8. Results of the experimental measurement of the proposed actuator subjected to sinusoidal inputs at (a) 1 Hz, (b) 3 Hz, (c) 5 Hz, and (d) 10 Hz.

5. CONCLUSION

This article has presented the design, modeling and experimental evaluation of a novel design for a miniature haptic actuator based on the tunable yield stress of electrorheological fluids. The device was designed in flow mode to minimize actuator thickness and mechanical complexity. An analytical model for the actuator's force output was derived and implemented into a numerical simulation. A prototype actuator was fabricated and tested experimentally using a dynamic mechanical analyzer. The resistive force generated by the actuator along its stroke was measured for both kinesthetic and vibrotactile input voltage signals. The experimental results verified those produced by the model. The results indicated that the actuator's resistive force increases with increased indentation depth and applied voltage. Furthermore, the measured results demonstrate distinct force rates that may be perceived by humans as a range of kinesthetic sensations in application. The vibrotactile performance of the actuator showed significant improvement over previous iterations. Thus, the actuator was confirmed capable of conveying a range of haptic feedback sensations. Future work will include embedding a thin pressure sensor and feedback control to act as a haptic interface by generating realistic sensations between a user and virtual environment.

ACKNOWLEDGMENTS

This work was supported by The Korea National University of Transportation.

REFERENCES

Adams RJ, Moreyra MR and Hannaford B (1998) Stability and Performance of Haptic Displays : Theory and Experiments. In: *Proceedings ASME International Mechanical Engineering Congress and Exhibition*, Anaheim, 1998, pp. 227–234.

An J and Kwon D-S (2002) Haptic Experimentation on a Hybrid Active/Passive Force Feedback Device. In: *Proceedings 2002 IEEE International Conference on Robotics and Automation*, 2002, pp. 4217–4222.

An J and Kwon D-S (2006) Stability and performance of haptic interfaces with active/passive actuators - Theory and experiments. *International Journal of Robotics Research* 25(11): 1121–1136.

Bianchi M, Scilingo EP, Serio A, et al. (2009) A new softness display based on bi-elastic fabric. In: *Proceedings of Third Joint Eurohaptics Conference and Symposium on Haptic Interfaces for Virtual Environment and Teleoperator Systems*, 2009, pp. 382–383.

Bullough WA, Johnson AR, Hosseini-Sianaki A, et al. (1993) The electro-rheological clutch: design, performance characteristics and operation. *Proceedings of the Institution of Mechanical Engineers, Part I: Journal of Systems and Control Engineering* 207(2): 87–95.

Burton SA, Makris N, Konstantopoulos I, et al. (1996) Modeling the Response of ER Damper: Phenomenology and Emulation. *Journal of Engineering Mechanics* 122(September): 897–906.

Choi S-B and Choi Y-T (1999) Sliding mode control of a shear-mode type ER engine mount. *KSME International Journal* 13(1): 26–33.

Coles TR, Meglan D and John NW (2011) The role of haptics in medical training simulators: A survey of the state of the art. *IEEE Transactions on Haptics* 4(1): 51–66.

Fricke J (1993) Tactile Graphic Computer Screen and Input Tablet For Blind Persons Using an Electrorheological Fluid. 5222895. United States.

Fujita K and Ohmori H (2001) A new softness display interface by dynamic fingertip contact area control. In: *Proceedings of the 5th World Multiconference on Systemics, Cybernetics and Informatics*, 2001, pp. 78–82.

Han S-S, Choi S-B and Cheong C-C (2000) Position control of X-Y table mechanism using electro-rheological clutches. *Mechanism and Machine Theory* 35(11): 1563–1577.

Jansen Y, Karrer T and Borchers J (2010a) MudPad : Tactile Feedback and Haptic Texture Overlay for Touch Surfaces. *Proc. of ACM Int.Conf. on ITS*: 11–14.

Jansen Y, Karrer T and Borchers J (2010b) MudPad: localized tactile feedback on touch surfaces. In: *Proceedings of the 23nd Annual ACM Symposium on User Interface Software and Technology*, 2010, pp. 385–386.

Kim S, Kim P, Park C-Y, et al. (2016) A new tactile device using magneto-rheological sponge cells for medical applications: Experimental investigation. *Sensors & Actuators A: Physical* 239: 61–69.

Laycock S and Day A (2003) Recent Developments and Applications of Haptic Devices. *Computer Graphics Forum* 22(2): 117–132.

Mazursky AJ, Koo J-H and Yang T-H (2018) Experimental evaluation of a miniature haptic actuator based on electrorheological fluids. In: *SPIE 10595 Active and Passive Smart Structures and Integrated Systems*, Denver, CO, USA, 2018. SPIE.

Monkman GJ (1992) An Electrorheological Tactile Display. *Presence: Teleoperators and Virtual Environments* 1(2): 219–228.

Pang XD, Tan HZ and Durlach NI (1991) Manual discrimination of force using active finger motion. *Perception & Psychophysics* 49(6): 531–540.

Park J and Khatib O (2006) A haptic teleoperation approach based on contact force control. *International Journal of Robotics Research* 25(5–6): 575–591.

Pfeiffer C, Mavroidis C, Bar-Cohen Y, et al. (1999) Electrorheological Fluid Based Force Feedback Device. In: *Proceedings of the 1999 SPIE Telemanipulator and Telepresence Technologies VI*, 1999, pp. 88–99.

Phillips RW (1969) *Engineering Applications of Fluids with a Variable Yield Stress*. University of California at Berkeley.

Ryu S, Yang TH, Kim SY, et al. (2012) Design of a New Miniature Haptic Button Based on Magneto-Rheological Fluids. *IEEE International Conference on Automation Science and Engineering*: 1–4.

Ryu S, Koo J-H, Yang T-H, et al. (2015) Mechanical and psychophysical performance evaluation of a haptic actuator based on magnetorheological fluids. *Journal of Intelligent Material Systems and Structures* 27(14): 1967–1975.

Song A, Morris D and Colgate JE (2005) Haptic telemanipulation of soft environment without direct force feedback. In: *Proceedings of the 2005 IEEE International Conference on Information Acquisition*, 2005, pp. 21–25.

Srinivasan MA and Basdogan C (1997) Haptics in virtual environments: Taxonomy, research status, and challenges. *Computers & Graphics* 21(4): 393–404.

Taylor PM, Hosseini-Sianaki A and Varley CJ (1996) An electrorheological fluid-based tactile array for virtual environments. In: *Proceedings of 1996 IEEE International Conference on Robotics and Automation*, 1996, pp. 18–23.

Vemuri SH, Jhon MS, Zhang K, et al. (2012) New analysis of yield stress on giant electrorheological fluids. *Colloid and Polymer Science* 290(2): 189–192.

Wen W, Huang X, Yang S, et al. (2003) The giant electrorheological effect in suspensions of nanoparticles. *Nature Materials* 2. Nature Publishing Group: 727–730.

Wereley NM and Pang L (1998) Nondimensional analysis of semi-active electrorheological and magnetorheological dampers using approximate parallel plate models. *Smart Materials and Structures* 7: 732–743.

Whittle M, Atkin RJ and Bullough WA (1996) Dynamics of an Electrorheological Valve. *International Journal of Modern Physics B* 10(23–24): 2933–2950.

Xu L, Li Y, Han L, et al. (2018) A test of giant electrorheological valve in DC and square wave AC fields with different frequencies. *Journal of Intelligent Material Systems and Structures* 29(2): 250–254.

Yang T-H, Kwon H-J, Lee SS, et al. (2010) Development of a miniature tunable stiffness display using MR fluids for haptic application. *Sensors and Actuators A: Physical* 163(1). Elsevier B.V.: 180–190.

Yang TH, Koo JH, Kim SY, et al. (2017) Modeling and test of a kinaesthetic actuator based on MR fluid for haptic applications. *Review of Scientific Instruments* 88(3).